4.2.3.3 Planetary seismology

MARTIN KNAPMEYER

4.2.3.3.1 Introduction

4.2.3.3.1.1 Symbols used

Symbol	Definition
a	Rupture area aspect ratio
α	Thermal expansion coefficient
β	Gutenberg-Richter distribution slope
d	Layer thickness
DU	Digital unit (difference of 1 bit in digital data)
δ_N	Normal fault dip angle
δ_T	Thrust fault dip angle
Δt	Considered time span
$\Delta\sigma$	Static stress drop during seismic event
η	Seismic efficiency of lithosphere deformation
F	Fourier transform
H	Seismogenic lithosphere thickness
M_0	Seismic moment
M_{cum}	Cumulative seismic moment available in given time span
M_{max}	Largest possible seismic moment
M_{min}	Smallest considered seismic moment
MoI	Moment of inertia factor
M_W	Moment magnitude
μ	Shear modulus of lithosphere rock
N	Number of events in deep moonquake cluster
ν	Poisson ratio of lithosphere rock
ω	Angular frequency
Q_κ	Quality factor for pure dilatational deformation
Q_μ	Quality factor for pure shear deformation
R_P	Planetary radius
ρ	Density
σ	Standard deviation
$\dot{T}$	Lithospheric cooling rate
t_{max}	Maximum age of faults considered in seismicity model
v_P	P wave velocity
v_S	S wave velocity
x	Normalized radius
X_Fe	Molar iron content in mantle
z	Depth

4.2.3.3.1.2 Overview

Seismological experiments have been conducted on four terrestrial bodies: Earth, Moon, Mars, and Venus. The seismology of the Earth is described in a separate volume [84Lb and successors] and is discussed only very briefly here for comparison.

About eight years of continuous data were returned from the Apollo seismometers. These data unveiled a seismic behaviour of the Moon that is largely different from that of the Earth.

Seismometers were also installed on Venus and Mars, but did not provide a clear picture of the seismic activity, let alone the inner structure, of these planets.

The following sections describe the seismic experiments that were actually carried out for Venus, Moon, and Mars, the amount and nature of the seismic activity of these planets, and their interior structure as inferred from seismology or theoretical modelling. Models based on direct observation are available for Earth and Moon only; theoretical velocity models are cited for Mercury, Venus and Mars. In case of Mars, a theoretical model of its seismic activity is described. Interior structure and composition in general are described in Section 4.2.3.2.2 of this volume.

Seismology of the Sun and the giant planets is not described here. The seismic/acoustic accelerometer experiment CASSE on board of the Rosetta mission's PHILAE-Lander [07Sei] is also not discussed in this chapter, since its target body is not a terrestrial planet, but a comet.

Polynomial representation of velocity models

The polynomial representation of velocity models known from Earth standard models PREM [81Dzi] and IASP91 [91Ken] is adopted for the velocity models of Mars in order to obtain a more compact form. The Venus model was published in polynomial form.

Velocity is expressed as polynomial of the normalized radius

$$x = \frac{R_P - z}{R_P} \tag{1}$$

where z is the depth below the surface.

Polynomials were constructed from values at discrete depths using a least squares fit. Polynomial coefficients were rounded to a prescribed number of digits. The smallest possible polynomial degrees and the smallest possible number of significant digits were used in order to reduce the amount of digits to obtain a lossless compression of the model information. All physical discontinuities are preserved.

At the depths given in the original discrete models, the polynomials reproduce the input velocities and densities with a relative accuracy of 10^{-4} or better. This accuracy, however, is purely numerical and does not imply that the model predicts the real velocities to 10^{-4} . The velocities are unlikely to have more than 2 or 3 significant digits.

4.2.3.3.2 Mercury

Mercury has been visited by only two spacecraft so far, and these were not intended to deliver lander units. The three Mariner 10 flybys in 1974 and 1975 returned images of 45% of its surface [78Dun]. The Messenger flyby of January 2008 provided images from the hemisphere invisible to Mariner 10 [08Mel].

4.2.3.3.2.1 Expected seismicity

The mechanical structure of Mercury is that of a thin elastic/brittle outer shell enclosing a more movable interior [88Mel]. This outer shell shows tectonic features, mainly in the form of lobate scarps [03Sol]. These are thought to be the surface traces of large (20-500 km long [03Sol], up to 2 km displacement [02Wat]) thrust faults reaching depths up to 35-40 km [02Wat]. Lobate scarps are compatible with a 1-2 km radius change of Mercury since its origin [03Sol].

Suggested seismic sources active today may be tidal deformation, thermal stress and both natural and artificial impacts [03Log2]. Meteorite impacts may be a significant source of seismic waves, because typical impact speeds are ≈50 km/s, compared to ≈20 km/s on the Moon and ≈7 km/s on Mars [08Mel].

4.2.3.3.2.2 Velocity models

Velocity models based on compositional and thermodynamical modelling (Fig. 1) are constructed e.g. by [03Van] and [08Riv]. Two end-member models were constructed by [08Riv]. Crustal thickness, density and seismic velocities of the crust are prescribed.

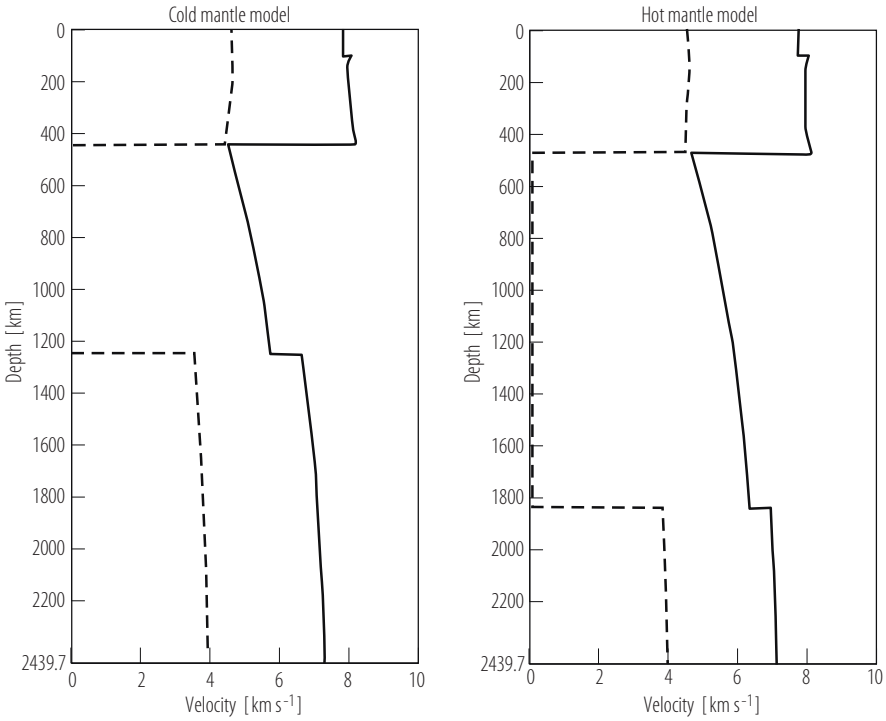

Fig. 1. Mercury velocity models of [08Riv]. Left: cold mantle after [91Spo], right: hot mantle after [06Bus]. Shear wave velocities are drawn as dashed lines, Compressional wave velocities as solid lines.

Table 1. Comparison of key properties of the "hot" and "cold" end member models of [08Riv].

Quantity	Hot mantle	Cold mantle
Crustal thickness [km] (fixed)	100	100
Crustal density [kg/m^3]	3000	3000
Core radius [km]	1960.436	1999.978
Inner core radius [km]	595	1200
Central temperature [K]	≈2500	≈2300
CMB temperature [K]	2000	1850

Table 2. Layering and range of velocities for each layer. Velocity variations are not linear with depth in both models, see Fig. 1. Models from [08Riv], communicated by [08Van]. Layer boundary depths are rounded to integer kilometres.

Layer	Hot mantle			Cold mantle		
	z [km]	V_S [kms^{-1}]	V_P [kms^{-1}]	z [km]	V_S [kms^{-1}]	V_P [kms^{-1}]
Crust	0 - 100	4.55	7.8	0 - 100	4.55	7.8
Mantle	100 - 440	4.43 - 4.66	7.95 - 8.06	100 - 479	4.47- 4.64	7.91 - 8.11
Outer core	440 - 1240	0	4.66 - 6.39	479 - 1845	0	4.35 - 5.71
Inner core	1240 - 2440	3.78 - 3.87	6.98 - 7.12	1845 - 2440	3.56 - 3.96	6.59 - 7.23

4.2.3.3.3 Venus

4.2.3.3.3.1 Seismic experiments

A passive seismic experiment using an electromagnetic vertical seismometer has been conducted on the soviet Venera 13 and Venera 14 landers, with the goal to detect microseismic activity with amplitudes of order 1 μm [82Ksa]. The two landers were identical [83Mor]. The seismometer was part of the meteorological Groza-2 experiment [83Mor]. It was mounted outside of the spacecraft bus on the landing ring [82Ksa]. Data downlink was limited to time windows of 8 s duration, interrupted by alternating 200 s and 392 s periods in which no recording was possible. During these interruptions, trigger electronics counted any amplitude spikes exceeding 1 μm displacement [82Ksa].

Table 3. Venera 13 and 14 lander parameters

Mission	Parameter	Quantity	Ref.
Venera 13			
	Landing time	01. March 1982	83Mor
	Duration of surface activity	127 min	83Mor
	Latitude	7°30' S	82Ksa
	Longitude	303° E	82Ksa
Venera 14			
	Landing time	05. March 1982	83Mor
	Duration of surface activity	57 min	83Mor
	Latitude	13°15' S	82Ksa
	Longitude	310°09' E	82Ksa

Table 4. Groza-2 seismometer parameters. Sensitivity not corrected for instrument response [82Ksa].

Parameter	Quantity
Eigenfrequency [Hz]	≈26
Mass [kg]	0.88
channels	1 (vertical)
Resolution in high sensitivity mode [m]	$\approx 5\times10^{-9}$
Resolution in low sensitivity mode [m]	1.5×10^{-7}
Event counter trigger threshold [m]	8×10^{-7}
Max. operation temperature [K]	780

No event was detected by Venera 13, but two possible microseismic events were found in the Venera 14 data [82Ksa].

The dense atmosphere of Venus allows for surface waves or displacements at the epicenter to couple into the atmosphere and experience an exponential amplitude increase due to the pressure decay with altitude. Dissipation of acoustic energy as well as adiabatic temperature changes in pressure waves are detectable with infrared sensors theoretically [05Gar, 07Dro].

4.2.3.3.3.2 Seismicity

The conditions at the surface allow for brittle failure of rock [03Dra], but no seismicity is expected below 300 km depth [71Der]. A seismic experiment with a life time of 1 day might have a 70 % chance to record one quake with $M > 3.0$ and a 90 % chance to record two events with $M > 2.0$ [71Der]. A three sensor network with a life time of 6-12 months might detect 600 events of $M > 4.0$ [93Sto].

The Groza-2 experiment onboard Venera 14 resulted in the detection of two possible microseismic events. The first occurred ~950 s after landing and was detected by the trigger, but not recorded. Its

amplitude therefore exceeded the trigger level. The second one occurred about 1361 s after landing and did not exceed the trigger level, but a part of the waveform no later than 56 s after the first arrival (timing concluded from details of the event detection and recording mode, see [82Ksa]) was recorded. By comparison with Earth seismograms, [82Ksa] conclude that the sources of these events were < 3000 km away and suggest a connection with the volcanic areas Beta Regio and Theia Mons.

4.2.3.3.3.3 Velocity model

Based on assumptions on the chemical composition and several equations of state, [83Zha] derived a model of density and seismic velocities as function of depth (model reproduced in [92Zha]).

Table 5. Seismological model of Venus, excluding the crust. Crustal density is assumed to be 2800 kg m^{-3}, Planetary radius is R_P = 6050 km, normalized radius x [83Zha, 92Zha].

Layer	z [km]	ρ [10^3kgm^{-3}]	v_P [kms^{-1}]	v_S [kms^{-1}]
Upper Mantle	70-481	7.374	27.17	14.4
		$-4.146\,x$	$-19.74x$	$-10.4\,x$
Transition Zone	481-756	10.101	19.32	13.54
		$-6.871\,x$	$-10.59x$	$-9.21\,x$
Lower Mantle	756-2840	6.77	14.84	6.83
		$-2.467\,x$	$-0.074\,x$	$+2.65\,x$
		$-0.266\,x^2$	$-5.011\,x^2$	$-3.95\,x^2$
Core	2840-6050	11.742	9.98	-
		$-0.17\,x$	$-0.66\,x$	
		$-5.402\,x^2$	$-9.125\,x^2$	
		$-3.642\,x^3$	$-0.74\,x^3$	

4.2.3.3.4 Earth

Seismology of the Earth is discussed in [84Lb] and its successors. Here, we summarize briefly what is necessary for a comparison with the other terrestrial planets.

4.2.3.3.4.1 Seismicity

The size-frequency distribution of earthquakes can be approximated by a power law (Gutenberg-Richter-Distribution). Table 6 shows a summary of seismic moments extracted from the data base of the Global Centroid Moment Tensor (GCMT) Project for the years 1984-2004, which is based on [83Dzi] and is available at [06Cmt]. Annual updates of recent moment tensors are published in *Physics of the Earth and Planetary Interiors*.

The annual moment release varied between 1.89×10^{21} Nm in 1988 and 4.3×10^{22} Nm in 2004, with a median of 2.84×10^{21} Nm. The Sumatra-Andaman earthquake of 26th Dec. 2004 released 32% (3.9×10^{22} Nm) of the global moment release of these 21 years.

Table 6. Average number of events exceeding a given seismic moment (GCMT, 1984-2004), rounded to integer numbers. Catalog sensitivity threshold is implied by top two rows.

M_0 [Nm]	M_W (ca.)	Exceeding events per year
1×10^{15}	3.9	881
1×10^{16}	4.6	881
1×10^{17}	5.3	603
1×10^{18}	5.9	134
1×10^{19}	6.6	28
1×10^{20}	7.3	5
1×10^{21}	7.9	1
1×10^{22}	8.6	0

4.2.3.3.4.2 Velocity model

Many seismological Earth models were constructed using seismic travel times or eigenmodes alone. The Preliminary Earth Reference Model (PREM) [81Dzi] also uses radius, mass, and moment of inertia. These quantities are often the only constraints for interior structure in planetology. The model is defined in terms of cubic polynomials for compressional and shear wave velocities and density, and layerwise constants for attenuation. It consists of 7 main layers with a distinction of oceanic and continental crust. The constraints for the construction of PREM are given in table 7, for comparison with the amount of data usually available in planetology. The layer polynomials can be found in [81Dzi].

Table 7. Constraints for construction of PREM

R_P [km]	6371
Mass [kg]	5.974×10^{24}
MoI [1]	0.3308
Normal mode eigenfrequencies	>1000
Normal mode Q values	ca. 100
Summary travel time observations	ca. 500
Body wave arrival times	26000 events
	ca. 2×10^{6} P wave arrivals
	ca. 2.5×10^{5} S wave arrivals

4.2.3.3.5 Moon

During four Apollo landing missions, active and passive experiments were conducted in order to determine the shallow crustal structure at the landing sites and the overall structure of the lunar interior.

After a first period of data evaluation and interpretation during the 1970s and 1980s, interest renewed in the late 20th century, due to increased computer power availability.

4.2.3.3.5.1 Seismic experiments

Seismometers for passive seismic experiments were delivered to the Moon by Apollo missions 11, 12, 14, 15, and 16. On Apollo 12, 14, 16, and 17, active experiments were carried out using dedicated geophones. Data recording and downlink of the seismometers of Apollo 12 through 17 used the Apollo Lunar Surface Experiment Package (ALSEP) radio connection, which was independent of the landing module.

4.2.3.3.5.1.1 Apollo landing sites

Table 8. Apollo seismometer sites. The locations of the ALSEPs and the Apollo 11 Lunar Module were determined using Very Long Baseline Interferometry techniques by [00Dav].

Station	Landing area	Lat. [°N]	Lon. [°E]	Radius [m]
Apollo 11	M. Tranquilitatis	0.67408	23.47297	1735472
Apollo 12	Oc. Procellarum	–3.00942	–23.42458	1736014
Apollo 14	Fra Mauro Highlands	–3.64398	–17.47748	1736343
Apollo 15	Mt. Appenninus / Hadley Rille	26.13407	3.62981	1735477
Apollo 16	Descartes Highlands	–8.97537	15.49812	1737453
Apollo 17	Taurus-Littrow	20.19209	30.76492	1734814

4.2.3.3.5.1.2 Active experiments

Active experiments were conducted using long and short period seismometers, with controlled impacts of spacecraft parts as seismic source (Table 9), but also with geophone profiles (Apollo 14 and 16) and arrays (Apollo 17), using various explosive charges as source.

The ascent stages of the lunar modules of Apollo 12, 14, 15, 17 as well as the upper stages of the Saturn V vehicles were used as impactors. Precise time and location of the impacts were obtained from spacecraft telemetry, except for the Apollo 16 S4B stage, where a propulsion system leakage and a loss of tracking reduced the control over the impact [72Amr]. The impact position given in Table 9 for S4B-16 was estimated from evaluation of seismic data [72Amr].

Table 9. Artificial impact parameters, from [74Tok]. Impactor designations: "LM" is Lunar Module ascent stage, "S4B" is Saturn V third stage, and the two closing digits denote the mission. Impact angle is measured from horizontal. Times are those received on Earth. Mass differences are due to different amounts of remaining fuel and consumables.

Impactor	Mass [kg]	Velocity [kms^{-1}]	Impact angle [deg]	Date	Time [UT]	Latitude N [deg]	Longitude E [deg]
LM-12	2383	1.68	3.7	20. Nov 69	22:17:17.7	–3.94	–21.2
LM-14	2303	1.68	3.6	07. Feb 71	00:45:25.7	–3.42	–9.67
LM-15	2385	1.7	3.2	03. Aug 71	03:03:37.0	26.36	0.25
LM-17	2260	1.67	?	15.Dec.72	06:50:20.8	19.96	30.5
S4B-13	13925	2.58	76	05. Apr 70	01:09:41.0	–2.75	–27.86
S4B-14	14016	2.54	69	04. Feb 71	07:40:55.4	–8.09	26.02
S4B-15	13852	2.58	62	29. Jul 71	20:58:42.9	–1.51	–11.81
S4B-16	?	?	?	19. Apr 72	21:02:04 ± 4	1.3±0.7	–23.8±0.2
S4B-17	14487	2.55	55	10. Dec.72	20:32:42.3	–4.21	–12.31

On Apollo 14 and 16, two different types of active sources were used: a manually operated thumper and a mortar that was operated from Earth. The thumper was a hand-held device Containing 21 small explosives. These were fired in direct contact with the ground, every 4.6 m (Apollo 14), or 4.75 m (Apollo 16) [72Amr, 74Coo]. The mortar was a small rocket launcher device, containing four grenades with solid state rocket engines and different amounts of explosives. The Apollo 14 mortar was not used [71Amr]. From the Apollo 16 mortar, only three of four grenades were fired because the pitch angle of the mortar was out of range after shot 3 [72Amr]. On Apollo 17, 8 explosive packages were deployed during Lunar Rover traverses at distances between 100 m and 2700 m by the astronauts [73Kov].

The geophones (Table 10) of all missions were moving coil-magnet instruments, flat in velocity for frequencies above the eigenfrequency and up to about 100 Hz [71Kov]. The Apollo 14 and 16 geophones were placed on a linear profile, at distances 3, 49, and 94 m from the ALSEP central station [71Kov, 72Kov]. The four geophones of Apollo 17 were deployed in an equilateral triangular array, with one geophone at each corner and one inside the triangle. The base of the triangle (geophones 1 & 2) was

oriented in E-W direction, with a base length of 92.2 m. Geophones 3 and 4 were 26.6 m and 74.4 m south of the baseline mid point [73Amr].

Table 10. Geophone instrument characteristics. The table gives mean and standard deviation of the actual instruments of each mission.

Mission	Number of sensors	Eigenfrequency [Hz]	Generator constant [$Vm^{-1}s^{-1}$]	Resistance [Ohm]	Sampling rate [Hz]	Ref.
Apollo 14	3	7.37±0.19	245.2±4.5	6135±62	500	71Kov
Apollo 16	3	7.42±0.03	255.6±1.2	6169±69	500	72Kov
Apollo 17	4	7.36±0.04	236.8±1.8	6039±95	118	73Kov

4.2.3.3.5.1.3 Passive experiments

During Apollo missions 11, 12, 14, 15, and 16, four-component seismometers were installed at each landing site (3 LP and a vertical SP channel). The Apollo 11 instrument was designed for a short life time and failed during its third lunation [69Amr]. It is of minor importance for the passive seismic experiment and not considered any further here. Instruments of the other four missions were shut down by telecommand in September 1977 [79Bat].

The LP sensor could be used in two modes of operation: in flat mode, with an essentially flat frequency response in displacement from 0.1 Hz to 1 Hz, and in peak mode, in which the instrument had a 5.6 times better sensitivity (measured at 0.45 Hz). In this mode, the LP sensors operated as underdampened pendulums [80Vos].

Table 11. Apollo seismometer characteristics

Category	Quantity	Value	Ref.
System data	Total mass	11.5 kg	70Lat
	Diameter	23 cm	70Lat
	Height	29 cm	70Lat
	Power consumption	4.3 - 7.4 W	70Lat
	A/D conversion	10 Bit (0 - 1023 DU)	80Vos
	Sensor equilibrium	ca. 500 DU	80Vos
	Sampling rate	1/0.060377 Hz	80Vos
LP Sensor	Resonant period (flat mode)	15 s	70Lat
	Resonant period (peak mode)	2.2 s	70Lat
	Usable freq. range	0.004 - 2 Hz	70Lat
	Maximum sensitivity (displacement)	0.3 nm	70Lat
	Sensitivity at max gain	5×10^{-6} V/m	69Als
	Pendulum mass	0.75 kg	69Als
	Digital dynamic range	60 dB	69Als
SP Sensor	Resonant period	1 s	70Lat
	Usable freq. range	0.05 - 20 Hz	70Lat
	Maximum sensitivity (displacement, 1 Hz)	0.3 nm	70Lat
	Sensitivity at max. gain	5×10^{-6} V/m	69Als
	Peak sensitivity freq.	8 Hz	69Als
	Digital dynamic range	60 dB	69Als

Table 12. Apollo seismometer horizontal sensor orientations [80Vos, 74Apo], from N over E

Station	+*X* Azimuth [°]	+*Y* Azimuth [°]
Apollo 11	0	90
Apollo 12	180	270
Apollo 14	0	90
Apollo 15	0	90
Apollo 16	334.5	64.5

Table 13. Apollo seismometer operation. Activation times are time of initial downlink acquisition. In 1977, Stations A12, A15, A16 were commanded to standby, A14 to OFF [79Bat]. The A11 instrument failed to respond after the sunset of the 2nd lunar day [69Amr].

Station	Activation [UT]	Shutdown
Apollo 11	21.July 1969, 04:41	01. Sep. 1969
Apollo 12	19.Nov. 1969, 14:21	30. Sep. 1977
Apollo 14	05.Feb. 1971, 17:23	30. Sep. 1977
Apollo 15	31. July 1971, 18:37	30. Sep. 1977
Apollo 16	21.Apr. 1972, 19:38	30. Sep. 1977

4.2.3.3.5.2 Seismicity

The 2004 revision of the Apollo long period event catalog [04Nak] lists 12555 events in five major event classes (Table 14) that were defined based on visual inspection in the 1970s. Recent analyses [05Bul, 07Bul] have shown that there are still many unlisted events belonging to known source clusters.

Table 14. Lunar seismicity overview. Categorization and event count are from [04Nak], meteorite energy release from [89Obe], shallow moonquake energy release from [87Obe], deep moonquake energy release from [74Lam], thermal moonquake energy release from [75Coo].

Event type	Number	Energy release [J]	
		Largest event	Smallest event
Meteorite impact	1744	8.2×10^{11}	???
Shallow moonquake	28	6.9×10^{12}	3.1×10^{7}
Deep moonquake	6897	100	1
Thermal moonquake	266	1	0.1
Unknown type	3611	?	?

4.2.3.3.5.2.1 Meteorite impacts

During the operation of the ALSEP network from 1969 to 1977, a total of 1744 meteorite impacts (Table 15) was recorded by the long period seismographs [82Nak, 04Nak]. Meteorite impacts can be identified from the seismogram characteristics since they show emergent P arrivals and a long rise time until the amplitude maximum of the envelope is reached. Location of the impacts is difficult due to emergent P arrivals and S arrivals that are generally weak, compared to moonquakes [78Dor].

The amplitude of impact seismograms depends on impactor mass, speed, density and impact angle [91Obe]. Detected impactor masses range from 0.1 kg to 1000 kg (22.5 km/s impact velocity assumed) [78Dor]. Possible impact speeds range from 14.5 km/s to 22.5 km/s [75Due]. Impactors above 500 g can be detected on the LP channels (100 g acc. to [78Dor]), smaller objects are visible on the SP channel and geophones only [75Due]. Impacts larger than 10 kg are detectable on the entire surface of the Moon [78Dor]. The influx of meteorite mass per year and km^2 of lunar surface was estimated by [75Due] to be

$$\log n(M) = -1.12 - 1.13 \log M \qquad (2)$$

for impactors with masses between 0.5 kg and 50 kg, where M is the impactor mass in gram and $\log(n(M))$ is the number of impacts with mass exceeding M. The largest detected impact (04. May 1975) might have created a crater of 53 m diameter, if the impact occurred vertically [89Obe].

The influx of kinetic energy due to meteorites was estimated by [89Obe] to be

$$\log_{10} n(E) = -0.99 \log_{10} E + 11.3 \quad (3)$$

for impactors with energies between 2×10^{11} J and 2×10^{12} J, where E is the impact energy in Joule and $n(E)$ the number of events with energy larger than or equal to E.

About 20 % of all impacts occur in only 3 % of the time [82Nak], with large falls concentrating between April and July [78Dor]. Seismic data reveals several known streams: the η Aquarides, Perseides, Northern and Southern δ Aquarides, Orionides, Leonides, and Geminides [91Obe]. Some swarms detected on the Moon, however, could not be correlated with any known meteor shower [91Obe].

4.2.3.3.5.2.2 Shallow moonquakes

The characteristic feature of the 28 shallow moonquakes is the extraordinary high SP-Z to LP-Z amplitude ratio, compared to meteorites and deep moonquakes. Hence they were originally termed "High-Frequency Teleseismic Events" (HFT Events) [74Nak].

Table 15. The 50 largest impacts observed by the Apollo Network. Magnitudes b are determined from spectral amplitudes at frequencies 0.5, 1.0, and 2.0 Hz. Energies and masses are estimated assuming 45° impact angle and 16.9 km/s impact velocity [89Obe], using the empirical relationship $\log_{10} E = 2b + 10.63546$ (simplified from [89Obe]) Location uncertainties σ were not determined for all events. Location for the first two listed events was ambiguous, therefore two solutions are given.

Year	DOY	Colatitude	σ	Longitude	σ	Mag. b	Energy [10^9 J]	Mass [kg]
71	143	a) 88.3	a) 0.07	a) –16.63	a) 0.07	–0.44	5.69	39.88
		b) 99.02	b) 0.08	b) –17.69	b) 0.06			
71	163	a)55.4	a) 0.17	a) 30.08	a) 0.51	0.62	750.69	5256.74
		b) 128.15	b) 0.25	b) -39.75	b) 0.48			
71	293	52.73	4.2	–40.52	7.11	0.1	68.46	479.42
71	304	134.9		39.9		–0.6	2.73	19.09
72	2	92.4		169.3		0.2	108.51	759.83
72	4	18		74.9		–0.6	2.73	19.09
72	132	95.5		–77.6		–0.4	6.85	47.94
72	134	89	0.59	–16.31	0.57	0.43	312.94	2191.37
72	168	126.8		–151.3		–0.3	10.85	75.98
72	199	54.02	13	135.03	16.38	0.51	452.33	3167.50
72	213	55.52	5.83	3.08	5.49	–0.29	11.36	79.56
72	242	105.5		86.2		–0.5	4.32	30.25
72	243	81.2		58.7		–0.6	2.73	19.09
72	248	84.9		–171.3		–0.2	17.20	120.42
72	321	92.4		–151.3		–0.4	6.85	47.94
72	324	24.24	2.19	–27.88	5.87	–0.41	6.54	45.78
72	337	16.2		181.2		–0.6	2.73	19.09
72	341	128		185.5		–0.2	17.20	120.42
73	82	15.5		–70.1		–0.6	2.73	19.09
73	113	144.57	7.22	31.41	8.74	–0.08	29.89	209.27
73	201	124.9		109.3		–0.3	10.85	75.98
73	213	70.5		–113.2		–0.6	2.73	19.09
73	262	166.96	0.2	–70.12	2.07	–0.33	9.45	66.18

Year	DOY	Colatitude	σ	Longitude	σ	Mag. b	Energy [10^9 J]	Mass [kg]
73	358	152.4		–111.3		–0.6	2.73	19.09
74	38	147.4		–83.2		–0.5	4.32	30.25
74	305	148		29.3		–0.4	6.85	47.94
74	325	97.57	0.58	25.02	0.74	–0.28	11.90	83.31
75	60	99.3		–96.3		–0.2	17.20	120.42
75	64	145.5		–61.3		–0.3	10.85	75.98
75	85	99.3		–80.7		–0.4	6.85	47.94
75	86	116.8		–118.2		–0.4	6.85	47.94
75	102	86.78	0.92	38.18	1.54	0.3	171.97	1204.25
75	111	68.7		–65.1		–0.5	4.32	30.25
75	124	128.17	3.64	–118.96	5.2	0.64	823.11	5763.90
75	168	84.9		–138.8		0	43.20	302.49
75	177	71.8		134.9		–0.3	10.85	75.98
75	256	148.7		67.4		–0.5	4.32	30.25
75	322	63.7		159.9		0.1	68.46	479.42
76	13	131.82	2.28	79.11	3.59	0.45	343.13	2402.79
76	21	41.2		129.9		0.1	68.46	479.42
76	25	93.21	3.35	–72.99	2.62	0.55	543.83	3808.17
76	109	32.4		–82		–0.1	27.26	190.86
76	137	100.42	13.8	15.3	4.49	–0.25	13.66	95.66
76	149	106.2		-8.2		–0.5	4.32	30.25
76	230	99.3		134.9		0	43.20	302.49
76	319	76.27	6.54	–89.84	8.83	0.64	823.11	5763.90
77	107	113.17	6.11	–70.27	3.5	0.1	68.46	479.42
77	179	120.5		–85.1		–0.2	17.20	120.42

On the basis of arrival times and coda of the then known 13 HFT events, [77Nak] concluded that the focal depth must be above 300 km depth, and even a depth below 100 km is considered unlikely. After consideration of the variation of the SP envelope and the arrival times of all 28 known events, [79Nak] revised this estimate to the interval 50-200 km.

The shallow moonquakes are among the strongest seismic events on the Moon, with seismic moments above 10^{12} Nm and moment magnitudes above 2.3 [87Obe] (the magnitude given by [87Obe] are body wave magnitudes, whereas [79Nak] uses a special HFT-Magnitude scale based on the digital units amplitude of the SP-Z sensor. Moment magnitudes given here and in Table 17 are derived from the seismic moments of [87Obe] using the relation $M_W = 2(\log M_0 - 9.1)/3$ [02Bor]).

It has been suggested that their occurrence is connected to the borders of the large impact basins [79Nak], and that they predominantly occur in the north-eastern and south-western quadrants of the lunar surface [79Nak]. [85Shi] found that HFT occurrence times correlate with the geocentric ecliptical longitude of the Moon. This was rediscovered by [06Fro], who used basically the same statistical test as [85Shi]. [06Fro] also claim that the location of the HFT also correlates with the geocentric ecliptical longitude: HFT events seem to occur on that part of the lunar surface which points to constellations Leo and Virgo. The range of physical explanations for the source mechanism comprises meteoroid impacts on extraordinary competent material [77Nak], impact basin rim tectonics [79Nak], release of thermal stresses remaining from an initially molten Moon [85Bin, 87Obe], planetary tides [85Shi], and deeply penetrating impacts of extrasolar particles of exotic types of matter [06Fro]. Stress drops of up to 210 MPa support the hypothesis of an initially molten Moon [87Obe], but care should be taken with interpretations as long as the source mechanism is unknown and the source depth uncertain.

The list of HFT locations based on velocity model LM-761 of [76Nak] is the only one containing all 28 events, but a recent relocation of eight HFT by [03Log] resulted in shifts of several degrees. LM-761 was a preliminary velocity model with features not maintained in newer models, like a strong negative gradient in shear wave velocity.

Table 16. Locations of the shallow moonquakes [79Nak]. Origin times and epicenters were estimated using model LM-761 [76Nak], assuming 100 km source depth. Location of events 3 is ambiguous. Location of event 15 could be constrained only to be at azimuth 30° from Apollo 16.

No.	Date	Time	Longitude [°N]	Latitude [°E]
1	17.04.1971	07:00:55	48	35
2	20.05.1971	17:25:10	42	–24
3	11.07.1971	13:24:45	43 or -42	–47 or –60
4	02.01.1972	22:29:40	54	101
5	17.09.1972	14:35:55	12	46
6	06.12.1972	23:08:20	51	45
7	09.12.1972	03:50:15	–20	–80
8	08.02.1973	22:52:10	33	35
9	13.03.1973	07:56:30	–84	–134
10	20.06.1973	20:22:00	–1	–71
11	01.10.1973	03:58:00	–37	–29
12	23.02.1974	21:16:50	36	–16
13	27.03.1974	09:11:00	–48	–106
14	19.04.1974	13:35:15	–37	42
15	29.05.1974	20:42:15	?	?
16	11.07.1974	00:46:30	21	88
17	03.01.1975	01:42:00	29	–98
18	12.01.1975	03:14:10	75	40
19	13.01.1975	00:26:20	–2	–51
20	13.02.1975	22:03:50	–19	–26
21	07.05.1975	06:37:05	–49	–45
22	27.05.1975	23:29:00	3	–58
23	10.11.1975	07:52:55	–8	64
24	04.01.1976	11:18:55	50	30
25	12.01.1976	08:18:05	38	44
26	06.03.1976	10:12:40	50	–20
27	08.03.1976	14:42:10	–19	–12
28	16.05.1976	12:32:40	77	–10

Table 17. Seismic moments and stress drops [87Obe]. The values given for corner frequency, energy release and static stress drop are lower boundaries. Moment magnitudes are derived from seismic moments. Corner frequency of event 28 is from [85Bin].

No.	Corner freq. [Hz]	Seismic moment [Nm]	Energy release [J]	Stress drop [MPa]	M_W
1	12	4.4×10^{14}	9.2×10^{11}	100	3.70
2	12	6.6×10^{13}	2.1×10^{10}	15	3.15
3	8	5.2×10^{13}	3.8×10^{9}	3	3.08
4	10	2.3×10^{14}	1.5×10^{11}	30	3.51
5	10	1.1×10^{13}	3.4×10^{8}	1.5	2.63
6	10	1.9×10^{13}	1.0×10^{9}	2.5	2.79
7	8	1.2×10^{13}	1.9×10^{8}	1	2.65
8	8	5.5×10^{12}	4.3×10^{7}	0.5	2.43
9	12	6.6×10^{14}	2.1×10^{12}	150	3.81
10	12	1.3×10^{14}	8.0×10^{10}	30	3.34
11	8	3.4×10^{13}	1.6×10^{9}	2	2.95
12	8	4.7×10^{12}	3.1×10^{7}	0.3	2.38
13	8	1.5×10^{13}	3.3×10^{8}	1	2.72

No.	Corner freq. [Hz]	Seismic moment [Nm]	Energy release [J]	Stress drop [MPa]	M_W
14	8	1.0×10^{13}	1.5×10^{8}	0.5	2.60
15	8	6.3×10^{13}	5.6×10^{9}	4	3.13
16	12	2.5×10^{14}	3.0×10^{11}	55	3.53
17	10	1.6×10^{15}	6.9×10^{12}	210	4.07
18	12	1.1×10^{14}	5.8×10^{10}	25	3.29
19	12	1.0×10^{13}	5.3×10^{8}	2.5	2.60
20	12	1.9×10^{13}	1.8×10^{9}	4	2.79
21	10	2.9×10^{13}	2.4×10^{9}	4	2.91
22	10	2.3×10^{13}	1.5×10^{9}	3	2.84
23	12	4.8×10^{13}	1.1×10^{10}	10	3.05
24	10	4.2×10^{13}	5.0×10^{9}	5	3.02
25	10	1.1×10^{14}	3.6×10^{10}	15	3.29
26	10	3.0×10^{14}	2.6×10^{11}	40	3.58
27	12	5.6×10^{13}	1.5×10^{10}	13	3.10
28	10	1.3×10^{13}			2.68

4.2.3.3.5.2.2 Deep moonquakes

The deep moonquakes group in 316 known clusters [04Nak] of repeating sources. For 106 of them, a linearized least squares location could be obtained from P and S wave arrival readings [05Nak]. The depth distribution peaks at about 950 km (Fig. 2). With few exceptions (clusters 29, 33, 218, 241, 244, 245, 282, 285), best fitting locations are all situated on the lunar near side [05Nak]. In several cases, the location process did not converge without fixing the focal depth prior to the location [05Nak]. Locations may be flawed by reading errors of tens of seconds [05Nak] and inadequate starting solutions.

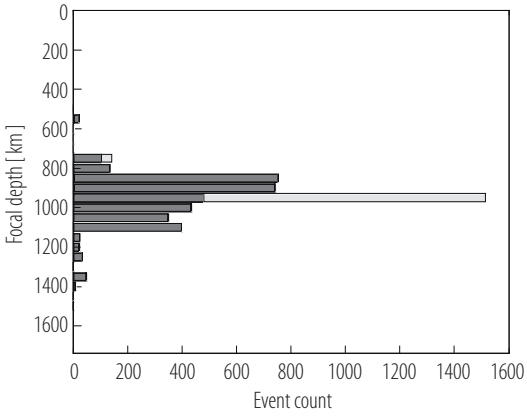

Fig. 2. Depth distribution of located events, based on [04Nak] clusters and [05Nak] locations. Depth bin width 50 km. Gray: locations with depth resulting from inversion, white: depth fixed manually.

The occurrence of deep moonquakes correlates strongly with monthly cycles of tidal deformation. This has been recognized from the first detections of moonquakes onward, since a possible correlation with the passage of the perigee was hypothesized [07Mei]. A spike train Fourier analysis [e.g. 07Bul] of the quake occurrence times gives the spectrum of event occurrence shown in Fig. 3.

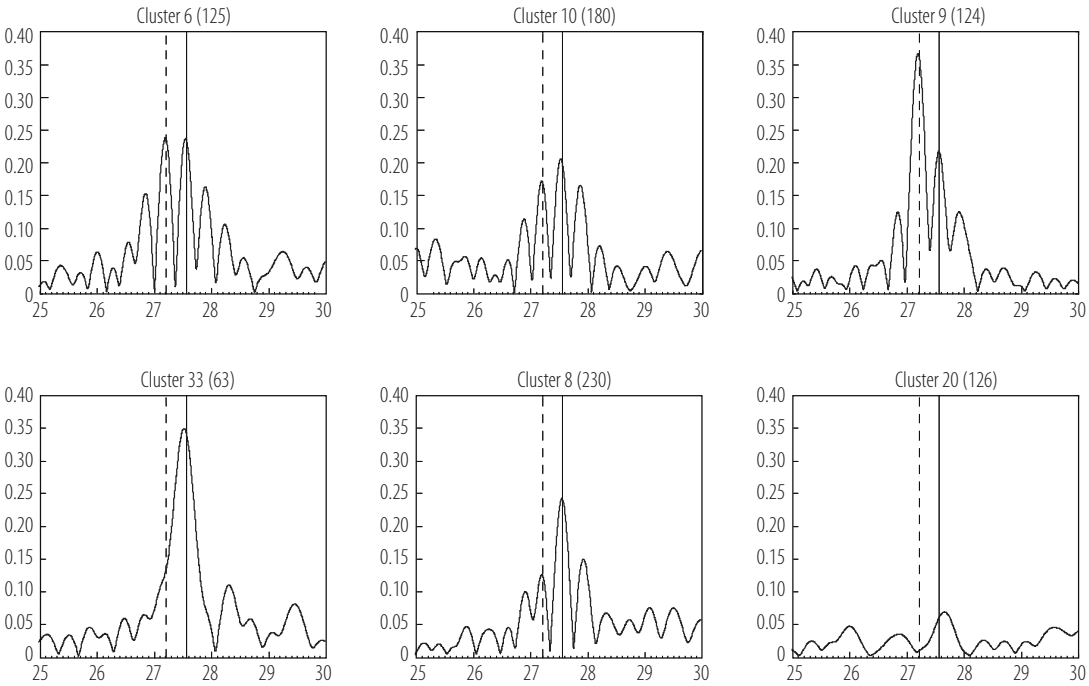

Fig. 3. Spectral analysis of deep quake occurrence. A spike train Fourier transform, normalized by the number of events contained in each cluster, is shown as function of period in days. Dashed vertical line: draconic month period, solid vertical line: anomalistic month period. Spectra computed following [07Bul], but with event assignment to clusters as in [04Nak].

The spectra show strong peaks at the periods of the draconic and anomalistic months (mean durations: 27.212221 and 27.554550 days [99Aa]). The synodic cycle does not appear in the spectra. The relative amplitudes of the draconic and anomalistic month vary between clusters. Clusters 6 and 10, show almost equal amplitudes for both, whereas cluster 9 prefers the draconic cycle. Clusters 8 and 33 prefer the anomalistic period. Cluster 20 does not show significant monthly cycles, because it consists of two subclusters which have near monthly activity periods, but are about 180° apart in phase (Fig. 4). The strongest spectral contribution in the spectrum of cluster 20 therefore is at half the period of the draconic month [07Bul].

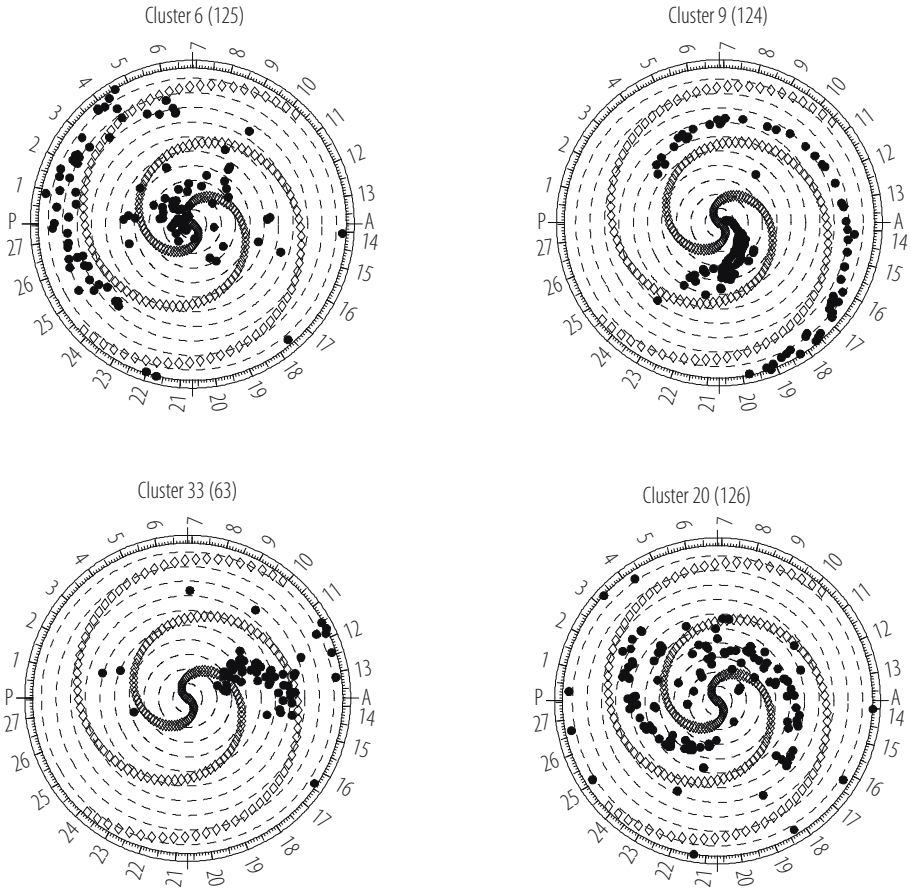

Fig. 4. Phase of deep quake clusters in relation to perigee, apogee and orbital nodes. Each dot represents the detection of a single deep quake. The angular coordinate is the number of days since the last lunar perigee passage, assuming a mean anomalistic month duration of 27.554551 days. "P" denotes the perigee, "A" denotes the apogee. The radius is the number of perigee passages since 29.06.1969, the last perigee before the landing of Apollo 11. Dashed concentric circles are drawn every 10 months. The two spirals of diamond symbols denote the time of passages through the ascending and descending nodes, respectively, assuming a mean draconitic month of 27.212220 days and starting with 22.09.1968, the last total eclipse of the sun before the landing of Apollo 11. The number of events belonging to each cluster is given in brackets in the figure headings. Cluster 6 is predominantly active in the two weeks surrounding the passage of the perigee. Cluster 9 shows an activity that is related very closely to the passage of orbital nodes, corresponding to a weak spectral component of the anomalistic month. Cluster 33 is an example for a strong anomalistic and a weak draconitic component. It's activity is highly correlated to the passage of the apogee. The activity of cluster 20 follows a two-armed spiral pattern, denoting seismic activity connected to passage of both the ascending and the descending node of the orbit, as suggested by the bi-weekly periodicity.

Table 18. Deep moonquake cluster locations, from [05Nak]. Uncertainty 1σ reflects [83Nak] velocity uncertainty, not arrival time uncertainty. Depth z = 933±109 km is assumed if depth could not be determined from data. For Clusters 59 and 60, z = 750±109 km was assumed.

Cluster	Lat. [°N]	σ [°]	Lon. [°E]	σ [°]	Depth [km]	σ [km]
1	–15.7	2.4	–36.6	4.6	867	29
3	–2.9	1.7	–50.3	6.3	946	22
5	1.1	94.2	–44.7	16.4	933	109
6	43.5	2.9	55.5	9.5	844	33
7	25	1.7	53.2	8	893	27
8	–23.7	4.8	–35.5	6.5	1086	37
9	–6	2.4	–19.7	3.6	1037	68

Cluster	Lat. [°N]	σ [°]	Lon. [°E]	σ [°]	Depth [km]	σ [km]
10	–35.7	4.9	–40.3	6.7	988	21
11	9.2	1.5	17.5	4.9	1187	87
13	–19.1	3	–41.7	5.6	973	23
14	–29.6	9.3	–44.4	7.8	933	109
15	0.7	0.7	–3.9	0.6	747	62
16	7.5	0.8	6.3	1.5	1019	78
17	25.5	2.3	–21.9	2.8	807	40
18	23.3	2.4	32.7	5.5	925	44
19	27.7	3	34.4	6.4	974	42
20	23.7	2.5	–31.4	5.3	945	50
21	–18.2	3	–50.8	7.2	1037	20
22	21.6	1.8	43.6	5.9	788	29
25	35.1	2.2	59.8	9.9	924	28
26	14.3	2.6	5.2	2	1122	90
27	23	3.3	20.4	4.7	1085	64
28	8.1	1.3	10.3	2.6	933	109
29	53.4	15.2	60.9	66.1	1077	32
30	12.7	1.2	–35.7	4.8	931	39
32	25	2.7	43.6	7.3	944	38
33	5.1	2.6	115.8	9.3	877	112
34	6.8	0.7	–7.2	1.3	971	77
35	5	1.5	36.1	11.4	933	109
36	27.5	4.7	–4.6	1.9	1058	74
37	22.5	5.5	29.7	10.7	1343	82
38	7.8	1.3	43.3	7	1031	37
39	–21.9	21.1	–12.7	5.1	933	109
40	–1.3	1.2	–10.3	1.5	867	66
41	13.8	1.3	–29.2	3.9	847	45
42	22.2	1.5	–50.7	6.8	907	28
44	50.2	2.9	60.2	12	908	37
49	8.6	4.6	–50.8	5.6	952	93
50	8.7	1	–53.4	5	828	27
51	12.3	1.4	37.7	8	1125	56
53	–10.1	39.9	–39.2	8.1	933	109
54	13.1	30.1	–52.4	10.8	933	109
56	1.1	1.6	–20.6	5	933	109
59	–9.5	17.6	–53.6	5.9	750	109
60	24.1	9.5	–52.2	8	750	109
64	30.1	2.9	53.2	9.8	975	24
65	46.6	3.9	42.3	8.2	861	25
70	34.8	2.1	63	11.3	1014	26
71	–20.9	22.1	–16.8	6.3	933	109
73	21.1	1.7	–44	5.6	908	28
74	34.7	2.5	60.1	10.6	1043	30
77	24.6	8.4	–23.4	11.1	1419	96
82	27.5	9.9	34.3	20.6	919	160
86	–40.9	7.5	–40.6	8.4	933	109
96	6.2	0.6	11.9	1.8	794	64
97	–8.4	2.9	17.9	3.8	989	71
99	10	1.1	22.8	4.2	989	69
100	–2	4.2	32.2	17.1	920	184

Cluster	Lat. [°N]	σ [°]	Lon. [°E]	σ [°]	Depth [km]	σ [km]
107	41	2.5	53.4	7.7	893	34
114	15.5	1.2	55.6	7.5	755	44
201	–40.6	14.8	–3.8	1.6	862	88
202	1	1.7	2.8	1.5	919	170
203	0.5	2	47.3	11.8	1243	50
204	–28.4	8.9	–66.6	9.2	933	109
209	–26.5	12	–35.1	7.2	933	109
212	12.8	1.4	–36.2	5.6	963	45
216	–13.7	3.9	–21.6	4.5	764	81
218	–2.4	4.4	–73.3	32.3	878	107
223	36.1	12.2	–2.4	1.3	863	145
224	–50.7	7.9	–21.4	5.5	933	109
230	6.3	0.9	22.1	9.7	855	188
231	34.3	12	45	29.9	933	109
233	24.1	5.1	26.1	8.2	933	109
234	36.8	4.5	21.2	4.5	1006	41
236	–7.8	3.5	5.4	1.7	933	109
237	12.2	1.9	3.5	1.5	933	109
238	26.3	8.7	20	9.8	831	169
239	26.7	5.6	5.2	2.1	933	109
241	–69.4	4.4	75.4	24.6	933	109
242	58.6	4.6	54.2	15.5	1025	31
243	7	1.3	8.3	4.1	1019	191
244	34.6	20.9	56.1	81	933	109
245	8.6	4.9	73	69.5	933	109
246	19.4	2.7	24.3	5.1	959	68
248	5.3	1.1	3.6	1.5	933	109
249	–3.4	2.5	12.5	3.1	933	109
250	–3.6	2.8	21.5	5.7	933	109
251	–46.5	8.3	38.9	9.3	933	109
255	1.4	1.6	15	3.7	933	109
257	35	6.2	19.1	5.5	1063	63
258	–7.1	3.5	15.3	4	933	109
259	3.4	0.6	2	0.7	559	97
260	–1.7	2.3	18	4.5	933	109
267	–7.6	5	36.7	13.2	933	109
271	53.8	6.8	35.2	19.2	933	109
272	–50	7.5	53.2	12.2	933	109
276	–3.7	3.6	–33.9	12.4	933	109
279	4.4	1.2	–4.7	1.8	933	109
280	2.4	2.7	46.1	20.2	933	109
281	–53.2	4.6	–54.4	11.4	933	109
282	15.5	2.4	97	12.3	1141	74
283	7.1	1.2	22.5	4.7	984	76
285	42.9	3.7	110.9	14.2	933	109
286	54.2	6.5	56.5	14	933	109
287	24.8	5.7	35.7	13.5	933	109
290	10.6	1.6	6.4	1.9	933	109

4.2.3.3.5.2.3 Thermal moonquakes

Thermal moonquakes are high frequency events in the vicinity of the seismometer, registered on the SP channels only. Their activity begins about 48 h after sunrise and decreases fast after sunset [74Lam]. They show repeating signals that can be grouped into highly localized source clusters. Each cluster shows an individual type of high correlation with the diurnal cycle. A thermal origin was thus concluded [74Lam]. Since the diurnal temperature wave decays very quickly with depth in the lunar soil, the events must occur close to or at the surface [75Coo]. Suggested mechanisms include thermal degradation of rocks and Apollo equipment [74Lam]. Consideration of the energy release makes booming dunes and small landslides likely sources [75Coo].

4.2.3.3.5.3 Velocity models

4.2.3.3.5.3.1 Shallow structure at landing sites

Seismic velocity models for the uppermost crustal layers at Apollo 14, 16, and 17 sites suggest a layered regolith structure with different degrees of fracturing and compaction. At the Apollo 14 and 16 sites, firm layer thicknesses could be given only for two layers reaching down to about 80 m (Table 19). Only the large profile lengths covered with the explosive packages of Apollo 17 allowed detecting a solid rock basement (Table 20).

Table 19. Apollo 14 and 16 landing site surface layering [71Kov, 72Kov]

Apollo 14			Apollo 16		
Layer	d [m]	v_P [kms^{-1}]	Layer	z [m]	v_P [kms^{-1}]
Regolith	8.5	0.104	Regolith	0 - 12.2	0.114
Fra Mauro formation	38-76	0.299	Cayley formation or impact debris	12.2 - ca. 82	0.250
Pre-Fra-Mauro material	?	?	Pre-Descartes material	> ca. 82	?

Table 20. Apollo 17 landing site surface layering [74Coo]

Apollo 17		
Layer	z [m]	v_P [kms^{-1}]
Regolith	0 - 4	0.100
Rubble/broken rock	4 - 32	0.327
Basaltic valley fill, fractured	32 - 390	0.495
Basaltic valley fill, less fractured	390 - 1385	0.960
Anorthositic highland breccia	> 1385	4.700

4.2.3.3.5.3.2 Global models

The discussion on the seismic velocity structure of the Moon is not yet settled. We here give an overview of models that were constructed in the first period of interpretation, during the 1970s and 1980s (Table 21), and from the second period in the early 2000s (Table 22). The more recent models result from extensive Monte Carlo modeling that could not be conducted in the early phase.

An important difference between the velocity models obtained in the two periods is that the recent models favor a crustal thickness of only 40 - 50 km [00Kha, 06Gag], whereas the earlier models concluded a crustal thickness of 60 km [81Goi, 82Nak]. The lower values are also supported by [06Che], who jointly determined the crustal thickness at the Apollo landing sites, sites of two artifical impacts and

sites of 19 meteorite impacts, using a bayesian Monte Carlo technique. Most impact sites were located in Mare areas, only two were at far side highlands. Individual members of the resulting model ensemble allowed for crustal thicknesses of up to 100 km at some of the 25 sites, but the best fitting solutions, typically give thicknesses of 25 - 50 km at the meteorite impact sites and 31 - 38 km at the Apollo landing sites. The highland crust appears to be 55 - 60 km thick. The crustal thicknesses estimated by [06Che] are also compatible with results from gravity inversion [06Che]. It must be taken into account, that [06Che] disregarded any lateral mantle variations, but attributed all travel time variations at the source and receiver sites. He might thus overestimate the thickness variation, especially concerning the far side sites.

The travel time data do hardly allow for the identification of seismic discontinuities within the Moon. The individual models therefore use different depth discretizations that are difficult to compare in tabular form. The tables given here do not try to regularize the depth sampling but to represent the models as they are. Earlier models than those reported here exist but are based on preliminary data sets.

The Toksöz et al. v_P model [74Tok] is based on the well known source times and positions of the artificial impacts.

The Bills & Ferrari model [77Bil] was intended mainly as a density and composition model. Seismic velocities were derived from density and elastic moduli. Velocities are given for top and bottom of each layer, with velocity discontinuities between layers. It explicitly defines a liquid core below 1400 km depth.

The model of Goins et al. [81Goi] contains a simplified crustal structure with constant velocity layers, and constant gradient layers for the mantle (linear interpolation between the given depth samples).

The model of Nakamura et al. [82Nak] defines constant velocity layers. The discontinuities between layers are not intended to represent mantle structure but are only discretization artifacts. The model indicates velocity uncertainties for layers below 58 km that are between 0.03 kms^{-1} for v_S at 58 - 270 km and 0.4 kms^{-1} for v_P below 500 km depth.

The more recent studies use Bayesian Monte Carlo inversion methods that produce a great number of models that are compatible with the observations. “Likely” velocity values and uncertainty boundaries are estimated from the ensemble of acceptable models. A representation in tables is therefore necessarily incomplete, since only averages and boundaries can be given.

The model of Khan et al. [00Kha] is a new inversion of the data used by [83Nak]. Uncertainties between 0.4 kms^{-1} (v_S at 45 km depth) and 2.1 kms^{-1} (v_P below 780 km depth) are reported. Table 22 gives the mean values only. The crustal thickness is deduced to be 45±5 km by [00Kha].

Gagnepain-Beyneix et al. [06Gag] have reprocessed data from artificial and meteorite impacts, shallow and deep quakes. They have tested the crustal structure and found compatibility with the thinner crust given by [00Kha], but do not give explicit crustal velocities above 28 km depth. Velocity uncertainties are significantly smaller than in [00Kha], which is mainly due to a different parameterization with fewer layers and fixed layer thicknesses. Only mean velocities are listed here.

Table 22. Recent global velocity models of the Moon. Depths are given in km, velocities in kms^{-1}. First columns is a layer count

Nr.	[00Kha]			[06Gag]		
	z	v_P	v_S	z	v_P	v_S
1	0	≈7.0	≈3.0	28 - 38	7.65	4.37
2	45	≈7.0	≈3.0	38 - 238	7.65	4.44
3	45	8.0	4.0	238 - 488	7.79	4.37
4	500	8.0	4.8	488 - 738	7.62	4.40
5	560	8.5	4.8	738 - 1038	8.15	4.50
6	560	9.9	5.9			
7	700	9.0	5.5			
8	780	11.0	6.0			
9	1100	11.0	6.0			

Table 21. Early global seismic velocity models of the Moon. Depths are given in km, velocities in kms^{-1}. First column is a layer count.

Nr	[74Tok]		[77Bil]			[81Goi]			[82Nak]		
	z	v_P	z	v_P	v_S	z	v_P	v_S	z	v_P	v_S
1	0	0.5	0	5.22	3.02	0-20	5.1	2.96	0 - 1	0.51	0.30
			20	5.22	3.02						
2	1	0.5	20	6.12	3.31	20-60	6.8	3.9	1 - 15	4.90	2.84
			70	6.52	3.51						
3	1	4.0	70	8.11	4.71	60	7.75	4.57	15 - 30	6.25	3.62
			300	7.89	4.39						
4	4	4.6	300	7.89	4.39	400	7.65	4.37	30 - 58	6.68	3.87
			800	7.80	2.89						
5	7	5.1	800	7.80	2.89	480	7.6	4.2	58 - 270	7.74	4.49
			1400	7.68	2.46						
6	10	5.4	1400	5.18	0	1100	7.6	4.2	270 - 500	7.46	4.25
			1740	5.22	0						
7	15	5.8							500 - 1740	8.26	4.65
8	20	6.1									
9	20.5	6.2									
10	21.25	6.72									
11	54.5	6.7									
12	57.5	8.2									
13	65	8.9									
14	200	8.8									

4.2.3.3.5.4 Attenuation

The long coda of all seismic events shows that intense scattering occurs, and from the coda in seismograms of meteorite impacts and deep moonquakes, one can conclude that there must be a zone of intense scattering and very low attenuation in the crust that might cover the entire Moon [74Lam]. Very weak S wave arrivals from far side impacts point to a zone of high attenuation in the deep interior in a zone with a radius of 600 to 800 km [74Lam]. Quantitative evaluations can be found e.g. in [74Dai] for the shallow crust and in [76Nak] for the mantle. See also [81Goi] and references therein.

In [80Bin] it was shown that a deep zone of high attenuation can explain the observed distribution of deep Moonquakes.

Seismic Q values differ from the tidally determined values, given e.g. by [81Yod] and [01Wil], which are averages of the entire Moon at frequencies much lower than the seismic frequencies. [01Wil] give separate Q values for periods between 10 days and 75 years.

Table 23. Attenuation model as summarized in [81Goi]. $Q_S = Q_P$ is assumed identical.

Region	z [km]	Q [1]
Crust	0…60	5000
Upper mantle	60…400	4000
Lower mantle	400…1000	1500
Attenuating zone	>1000	<500

4.2.3.3.6 Mars

4.2.3.3.6.1 Seismic experiments

Only one seismic experiment has been conducted on Mars so far, with one seismometer on each of the two Viking landers (Table 24) [77Coo]. The Viking 1 instrument failed to uncage. The instruments were mounted on top of the lander units, close to one of the three legs of the lander. It was therefore sensitive to noises generated by wind and lander-internal sources [77And].

The interpretation of martian seismograms is difficult because of the applied data compression [76And]: Only the absolute value of the 0.5 Hz low-pass filtered signal [77And] and a running count of positive zero crossings were sampled at 1.01 Hz and recorded at a resolution of 7 bits and 5 bits, respectively.

Based on the sensitivity of the instrument and assumptions on the attenuation in the martian interior, [79Goi] estimated that the Viking 2 instrument (Table 25) was not able to detect events with magnitude smaller than 9 from the Tharsis area (about 110° epicentral distance).

Table 24. Viking lander overview. Lander positions are with respect to an ellipsoid with 3397.2km equatorial radius and flatness 0.0105 [97Fol]. The missions ended with the last successful communications and cease of transmissions, respectively [92Sny].

	Viking 1	Viking 2	Ref.
Landing site	Chryse Planitia	Utopia Planitia	[92Sny, 77And]
Landing date & time [UTC]	20. July 1976, 11:53:06	03. Sep.1976, 22:37:50	[77Coo]
Seismometer uncaging	failed	04. Sep. 1976, 00:53:01	[77Coo, 76And]
End of experiment	-	2. Apr.1978	[79Tok]
Mission end	13. Nov. 1982	11. Apr.1980	[92Sny]
Latitude [°N]	$22.6969 \pm 7\times10^{-4}$	$48.2688 \pm 5\times10^{-4}$	[97Fol]
Longitude [°E]	$-48.2217 \pm 5\times10^{-4}$	$134.0100 \pm 6\times10^{-4}$	[97Fol]
Elevation [m]	-2690 ± 2	4230 ± 4	[97Fol]

Table 25. Viking seismometer characteristics [77And]. The raw sample stream ("initial") is downsampled according to the registration mode.

Category	Quantity	Value
System data	Total mass	2.2 kg
	Size	$12\times15\times12$ cm^3
	Power consumption	3.5 W
	Envelope	7 Bit
	A/D conversion	plus 1 sign bit
	Zero crossing count A/D conversion	5 Bit
	Buffer memory	2×2048 Bit
Sampling rates	Initial	121.21 Hz
	High data rate	20.2 Hz
	Normal mode	4.04/60 Hz
	Event mode	1.01 Hz
Sensor	Resonant period	4 Hz
	Usable freq. range	0.1 - 10 Hz
	Max. sensitivity	2 nm @ 3 Hz 10 nm @ 1 Hz
	Pendulum mass	16 g
	Generator const.	177 Vm^{-1}s^{-1}
	Vertical tilt tolerance	35°
	Horizontal tilt tolerance	23°

4.2.3.3.6.2 Observed seismicity

On sol 80 (i.e. 80 martian days after landing), an event was detected that was interpreted as a possible local Marsquake at 110 km distance after comparison with two terrestrial events recorded in Pasadena. No other candidate Marsquake was detected during the first 146 sols [77And]. Since no wind speed data are available for the time of detection [77And], it cannot be ruled out that the event is due to wind noise and not of tectonic origin.

From this amount of non-detection, [77And] concluded that the seismicity of Mars per unit surface area is lower than on Earth at a significance level of 95 %, but that the Viking data are not sufficient to determine if Mars is more active than the Moon. These estimates rely on Q being between 500 and 2000 in the martian interior [77And, 79Goi].

4.2.3.3.6.3 Expected seismicity

The annual seismic moment release of Mars was estimated to be larger than 10^{18} Nm by [92Gol] based on an evaluation of the total slip of faults visible on the martian surface. Later on, [02Gol] bracket the annual budget between 10^{17} Nm and 10^{19} Nm.

The most likely source of seismicity is thermoelastic stress due to secular cooling of the interior [91Phi]. [06Kna] refine the resulting seismicity estimate and add a model for spatial distribution, based on tectonic faults that are visible at the martian surface. The model is given by three equations, describing the cumulative seismic moment release per time (eq. 4), the size-frequency distribution (eq. 5), and the size of the largest event possible on a given fault (eq.6).

$$M_{cum} = \frac{4}{9}\pi\eta\mu\alpha\dot{T}\Delta t\frac{\left\lfloor R_{\mathrm{P}}^3 - (R_{\mathrm{P}} - H)^3 \right\rfloor^2}{\left(R_{\mathrm{P}} - H/2\right)^2} \tag{4}$$

$$N(M_0) = \frac{\left(M_{\min}/M_0\right)^{\beta} - \left(M_{\min}/M_{\max}\right)^{\beta}}{1 - \left(M_{\min}/M_{\max}\right)^{\beta}} \tag{5}$$

$$M_0(L) = \frac{2}{\pi}\frac{\Delta\sigma}{1-\nu} L \min\left(\frac{H}{\sin\delta}, \frac{L}{a}\right)^2 \tag{6}$$

The Moment-Length-Relation (6) is valid for $M_{\min} \le M_0 \le M_{\max}$. It is based on the constant static stress drop model and assumes a rectangular fault surface. The input parameters for the three equations are discussed in detail in [06Kna]. Five different scenarios are defined there as end members and middle of the likely parameter range (Tables 26 - 28). The distribution of tectonic faults visible in the MOLA digital topography model at a resolution of 64 pixel per degree [01Smi, 03Smi] is used to guide the distribution of epicentres over the martian surface, as shown in Fig. 4 for the “Medium” model.

Table 26. Seismicity model input parameters. Scenarios are distinguished by the cumulative Moment (strong, medium or weak) and the total number of events per year (few, medium or many).

Parameter	Unit	Scenario				
		Strong/Few	Strong/Many	Medium	Weak/Many	Weak/Few
R_P	[km]	3389.515	3389.515	3389.515	3389.515	3389.515
H	[km]	150	150	107	40	40
δ_T	[°]	25	25	25	25	25
δ_N	[°]	60	60	60	60	60
a	1	2	3	2.5	3	2
$\dot{T}$	[10^{-7}Ka^{-1}]	1.1	1.1	0.5	0.2	0.2
α	[10^{-5}K^{-1}]	3	3	2	2	2
μ	[GPa]	70	70	40	30	30
v	1	0.25	0.25	0.25	0.25	0.25
$\Delta\sigma$	[MPa]	10	3	5	3	10
η	1	1	1	1	0.5	0.5
M_{min}	[Nm]	3.981×10^{10}	3.981×10^{10}	3.981×10^{10}	3.981×10^{10}	3.981×10^{10}
M_{max}	[Nm]	3.36×10^{20}	3.42×10^{16}	2.41×10^{18}	3.42×10^{16}	3.37×10^{20}
β	[1/log(Nm)]	0.625	0.625	0.625	0.625	0.625
Δt	[a]	1	1	1	1	1
t_{max}	[Ga]	5	5	5	5	5

Table 27. Annual seismic moment. M_W is the moment magnitude of a single event that releases the entire annual budget. 50% of the parameter space correspond to models with an annual budget between 3.75×10^{17} Nm ($M_W = 5.65$) and 9.71×10^{17} Nm ($M_W = 5.925$). A fraction smaller than 10^{-7} of the parameter space are outside the "weak" and "strong" boundaries.

Model	M_{cum} [Nm]	M_W
Weak/Few	3.42×10^{16}	4.96
Weak/Many	3.42×10^{16}	4.96
Medium	5.99×10^{17}	5.78
Strong/Few	4.78×10^{18}	6.39
Strong/Many	4.78×10^{18}	6.39

Table 28. Predicted event recurrence times: mean time after which an event of given magnitude recurs, computed for entire planet. Empty fields are due to limitation of the strongest possible event.

M_W	Model				
	Strong/Few	Strong/Many	Medium	Weak/Many	Weak/Few
1	38 min	72 s	48.5 min	2.5 h	3.9 d
2	5.5 h	10.5 min	7 h	21.9 h	33.5 d
3	1.9 d	1.5 h	2.5 d	7.9 d	290 d
4	17.1 d	13.1 h	21.8 d	68.5 d	6.7 a
5	148 d	-	189 d	-	50 a
6	3.6 a	-	4.5 a	-	516 a
7	30.3 a	-	-	-	≈ 4500 a
7.6	115 a	-	-	-	≈ 17000 a

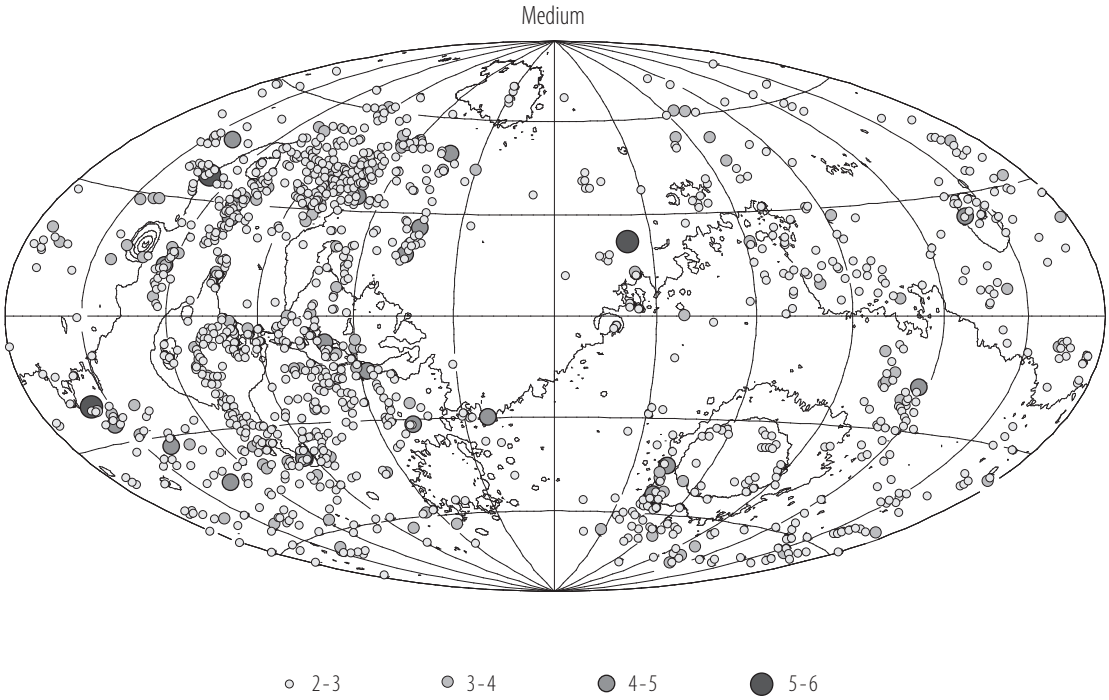

Fig. 5. Simulated epicentre distribution for the "Medium" scenario. Isohypses are drawn for elevations from –5 km to +20 km in steps of 5 km. Graticule is drawn with 30°×30° mesh width.

4.2.3.3.6.4 Velocity models

An overview of several models of the martian interior is given in Table 29.

Seismic velocity and density models can be built based on equations of state and a given chemical composition, as described in [97Soh, 05Soh] and Section 4.2.3.2.2 of this volume. [97Soh] have constructed models by solving the governing equations and using a chemical composition derived from the SNC meteorites and a Moment of Inertia Factor of $MoI = 0.366$. The Fe/Si = 1.35 ratio of the model in Table 30 deviates significantly from the bulk chondritic value of Fe/Si = 1.71 [97Soh]. It was not possible to construct a model that satisfies both the Moment of Inertia Factor and the chondritic Fe/Si ratio.

Model AR [78Oka] was constructed using a chemical composition derived from chondritic meteorites and using a MoI of 0.3654. Seismic travel times and eigenmode periods are given in [78Oka].

The models from [96Gud] were constructed to explore the value of spheroidal oscillation measurements for core radius determinations.

In [96Moc], the effect of the iron content of the martian mantle was studied: A higher Fe content increases density, but decreases seismic velocities. It also smoothes out the olivine α-β-transitions into gradient zones of a few hundred kilometres thickness, since an increased iron content in olivine allows the coexistence of the involved mineral phases. There is no β-γ-transition.

Different chemical models and recent high pressure / temperature data for mantle minerals of Mars have been used by [04Gud]. The structure and composition of the core were varied. A content of 50 mol% hydrogen in the core appears to be necessary to fit the chondritic Fe/Si ratio. [04Gud] also study the seismic source size necessary to excite higher order spheroidal free oscillation modes. Model M6 of [04Gud] best satisfies the MoI, but has a Fe/Si ratio of only 1.55.

The models of [05Zha] (Tables 31 and 32) satisfy the updated MoI and love number that resulted from Mars Global Surveyor. As in [04Gud], different compositions were used. The preferred model M13 has a Fe/Si ratio of 1.58. The crust of M13 was modelled separately and has a rather complex structure. Since the upper 10 km of the model are difficult to represent by compact polynomials, they are presented as discrete depth values as communicated by the authors.

Table 29. Comparison of Mars main discontinuity depths. The [96Gud] models define the olivine α-β-transformation only. None of the models has a Perovskite layer.

Model	Reference	Moho [km]	Olivine α-β [km]	Olivine β-γ [km]	Core [km]
A	97Soh	110	1030	1357	1922
B	97Soh	252	1058	1416	1723
AR	78Oka	50	1133	none	1694
M511L	96Gud	150	853.3	-	1711.9
M512L	96Gud	150	853.3	-	1834
M513L	96Gud	150	853.3	-	1928.9
M522L	96Gud	100	840.7	-	1823.8
M532L	96Gud	50	831.6	-	1827.2
M512H	96Gud	150	994.6	-	1817
M412L	96Gud	150	-	-	1834
X_{Fe}=10	96Moc	-	1130	1425	1852
X_{Fe}=20	96Moc	-	≈ 1000	(gradient)	1852
X_{Fe}=30	96Moc	-	≈ 1000	(gradient)	1852
X_{Fe}=40	96Moc	-	(gradient)	(gradient)	1852
M6	04Gud	50	1117	1413 - 1454	1728
M13	05Zha	50	1140	1439 - 1479	1691

Table 30. Seismic velocity model A of [97Soh], represented as polynomials of normalized radius x which reproduce the original values of [97Soh] with a relative accuracy better than 10^{-5} (this accuracy does not imply that the model predicts the real velocities to 10^{-4}. The velocities are unlikely to have more than 2 or 3 significant digits).

Layer	z [km]	v_P [kms^{-1}]	v_S [kms^{-1}]	ρ [10^3 kgm^{-3}]
Crust	0.000	+13.53241	−79.52797	−36.87198
	…	$-10.50178x$	$+277.3684x$	$+120.5534x$
	109.720	$+8.43717x^2$	$-322.57x^2$	$-121.4632x^2$
		$-3.808449x^3$	$+149.5597x^3$	$+40.58647x^3$
			$-20.80173x^4$	
Rheological lithopshere	109.720	+58.52484	+9.4101	+64.35302
	…	$-202.6362x$	$-14.47814x$	$-263.596x$
	335.220	$+317.4511x^2$	$+17.00685x^2$	$+426.1308x^2$
		$-223.4807x^3$	$-7.503172x^3$	$-304.0523x^3$
		$+58.13115x^4$		$+80.65374x^4$
Thermal lithosphere	335.220	+15.75339	−328.7083	+211.6707
	…	$-18.13458x$	$+1538.531x$	$-935.3949x$
	481.620	$+18.78073x^2$	$-2655.328x^2$	$+1575.777x^2$
		$-8.415148x^3$	$+2034.406x^3$	$-1179.016x^3$
			$-584.5912x^4$	$+330.5188x^4$
Olivine α layer	481.620	+11.92409	+6.594795	+2.588586
	…	$-4.863865x$	$-2.594216x$	$+7.297398x$
	1029.420	$+3.48065x^2$	$+1.654337x^2$	$-15.20067x^2$
		$-2.547134x^3$	$-1.29049x^3$	$+13.03664x^3$
				$-4.3209x^4$
Olivine β layer	1029.420	+11.15706	+8.333783	+4.402694
	…	$-0.9921897x$	$-13.17451x$	$-0.5597552x$
	1356.720	$-1.817251x^2$	$+27.4708x^2$	$+0.1313887x^2$
			$-28.73018x^3$	$-0.2796876x^3$
			$+10.84136x^4$	
Olivine γ layer	1356.720	+12.00398	+6.820569	+4.643348

Layer	z [km]	v_P [kms^{-1}]	v_S [kms^{-1}]	ρ [10^3 kgm^{-3}]
	…	$-4.233449x$	$-2.632441x$	$-0.9300214x$
	1887.220	$+3.625313x^2$	$+2.379488x^2$	$+0.7406889x^2$
		$-2.97074x^3$	$-1.905217x^3$	$-0.6193321x^3$
Lower thermal	1887.220	+65.41714	+9.928651	+6.495805
boundary	…	$-247.4658x$	$-16.47753x$	$-9.322339x$
Layer	1921.520	$+279.1924x^2$	$+16.95096x^2$	$+9.971156x^2$
Core	1921.520	+6.538969	0	+7.293911
	…	$+0.0038757x$		$+0.0014502x$
	3389.920	$-2.654013x^2$		$-1.846201x^2$
		$+0.2664053x^3$		$+0.1318379x^3$
		$-1.1473x^4$		$-0.6374107x^4$

Table 31. M13 upper crust, encompassing changes in petrology and porosity [05Zha].

z [km]	v_P [kms^{-1}]	v_S [kms^{-1}]	ρ [10^{3}kgm^{-3}]	z [km]	v_P [kms^{-1}]	v_S [kms^{-1}]	ρ [10^{3}kgm^{-3}]
0.000	0.75	0.5	1.6	4.407	3.137	1.602	2.936
0.339	0.9337	0.5848	1.835	5.424	3.688	1.856	3.057
1.017	1.301	0.7542	2.05	6.441	4.347	2.224	3.143
1.356	1.485	0.839	2.237	7.458	5.148	2.74	3.203
2.373	2.035	1.093	2.542	9.153	6.483	3.6	3.259
3.390	2.586	1.347	2.769	10.509	7.149	4.029	3.289

Table 32. M13 lower crust and mantle, represented as polynomials of normalized radius x, which reproduce the original values of [05Zha] with a relative accuracy better than 10^{-4} (This does not imply that the model predicts the real velocities to 10^{-4}. The velocities are unlikely to have more than 2 or 3 significant digits).

Layer	z [km]	v_P [kms^{-1}]	v_S [kms^{-1}]	ρ [10^{3}kgm^{-3}]
Crust	10.509…19.662	+3.8363	+0.71631	+12.9151
		$+3.3233x$	$+3.3233x$	$-9.64753x$
	19.662…21.357	+7.1395	+2.032	+3.319
			$+2x$	
	21.357…36.273	+4.88	+303.338	+19.2552
		$+2.273x$	$-606.47x$	$-31.8705x$
			$+307.189x^2$	$+15.9341x^2$
	36.273…37.968	+7.129	+4.007	+5.2996
				$-2x$
	37.968…49.833	+5.753	+2.631	+466.362
		$+1.391x$	$+1.3913x$	$-936.347x$
				$+473.364x^2$
Upper Mantle	49.833…1140.396	+10.8271	+6.06663	+5.72194
		$-3.02725x$	$-4.88816x$	$-8.24998x$
		$-0.440858x^2$	$+7.15595x^2$	$+13.4267x^2$
			$-5.96503x^3$	$-10.7005x^3$
			$+1.81681x^4$	$+3.14751x^4$
Olivine β layer	1140.396… 1194.636	+60.4045	+40.689	+20.7734
		$-116.615x$	$-82.623x$	$-37.402x$
		$+58.1449x^2$	$+42.517x^2$	$+17.4664x^2$
	1194.636…1439.055	+10.601	+5.219	+4.85878
		$-2.0564x$	$-0.3184x$	$-1.71744x$
				$+0.310413x^2$

Layer	z [km]	v_P [kms^{-1}]	v_S [kms^{-1}]	ρ [10^{3}kgm^{-3}]
Olivine γ layer	1439.055…1479.057	+19.0686	+12.7321	+12.726
		$-16.7687x$	$-15.9268x$	$-25.379x$
			$+4.43858x^2$	$+17.671x^2$
	1479.057…1579.401	+11.067	+5.735	−58.2623
		$-2.5733x$	$-1.011x$	$+341.552x$
				$-623.054x^2$
				$+378.207x^3$
	1579.401…1690.932	+11.087	+5.73	+4.3434
		$-2.6115x$	$-1.002x$	$-0.54932x$
Core	1690.932…2540.805	+5.8285	0	+7.40043
		$-9.48283x$		$-7.0115x$
		$+39.2734x^2$		$+28.73x^2$
		$-74.6938x^3$		$-54.1282x^3$
		$+43.8172x^4$		$+31.2134x^4$
	2540.805…3220.500	+4.986	0	+6.774
		$+0.9256x$		$+0.5809x$
		$-13.88x^2$		$-9.044x^2$
		$+72.45x^3$		$+48.07x^3$
		$-144.8x^4$		$-98.73x^4$
	3220.500…3390.000	+5.006	0	+6.786

Acknowledgements
The assistance of S. Hempel in the preparation of the lunar seismicity tables is gratefully acknowledged.

4.2.3.3.7 References for 4.2.3.3

69Als Apollo Lunar Surface Experiments Package Flight System Familiarization Manual, The Bendix Corporation, ALSEP-MT-03, revised version 15. Apr. 1969.
69Amr Apollo 11 Mission Report, NASA Manned Spacecraft Center, Houston, TX, MSC-00171 (1969).
70Lat Latham, G.V., et al.: NASA Manned Spacecraft Center, Houston, Texas, SP-235 (1970).
71Amr Apollo 14 Mission Report, NASA Manned Spacecraft Center, Houston, TX, MSC-04112 (1971).
71Der Derr, J.S.: Bull. Seis. Soc. Am. **61** (1971) 1731.
71Kov Kovach, R.L., et al.: NASA Manned Spacecraft Center, Houston, Texas, SP-272 (1971).
72Amr Apollo 16 Mission Report, NASA Manned Spacecraft Center, Houston, TX, MSC-07230 (1972).
72Kov Kovach, R.L., et al.: NASA Manned Spacecraft Center, Houston, TX, SP-315 (1972).
73Amr Apollo 17 Mission Report, NASA Lyndon B. Johnson Space Center, Huston, TX, JSC-07904 (1973).
73Kov Kovach, R.L., et al.: NASA Johnson Space Center, Houston, TX, SP-330 (1973).
74Apo Apollo Scientific Experiments Data Handbook; NASA Lyndon B. Johnson Space Center, Report JSC-09166, NASA Technical Memorandum TM X-58131, Washington D.C. (1974).
74Coo Cooper, M.R., Kovach, R.L.: Rev. Geophys. Space Phys. **12** (1974) 219.
74Dai Dainty, A.M., Toksöz, M.N.: The Moon **9** (1974) 11.
74Lam Lammlein, D.R., et al.: Rev. Geophys. Space Phys. **12** (1974) 1.
74Nak Nakamura, Y., et al.: Proc. Fifth Lunar Conf., Geochimica et Cosmochimica Acta, vol., 3, Suppl. 5, (1974) 2883.
74Tok Toksöz, M.N., et al.: Rev. Geophys. Space Phys. **12** (1974) 539.
75Coo Cooper, M.R., Kovach, R.L.: Proc. Lunar Sci. Conf. 6th, (1975) 2863.

75Due Duennebier, F., et al.: Proc. Lunar Sci. Conf., 6th. (1975) 2417.
76And Anderson, D.L., et al.: Science **194** (1976) 1318.
76Nak Nakamura, Y., et al.: J. Geophys. Res. **81** (1976) 4818.
77And Anderson, D.L., et al.: J. Geophys. Res. **82** 4524 (1977).
77Bil Bills, B.G., Ferrari, A.J.: J. Geophys. Res. **82** (1977) 1306.
77Coo Cooley, C.G., Lewis, J.G.: Martin Marietta Corp., Denver, Col., NASA CR-145148, 118pp. (1977).
77Nak Nakamura, Y.: Phys. Earth Planet. Int. **14** (1977) 217.
78Dor Dorman, J. et al.: Proc. Lunar Planet. Sci. Conf. 9th (1978) 3615.
78Dun Dunne, J.A., Burgess, E.: NASA SP-424, NASA JPL., Pasadena, CA, 234p. (1978).
78Oka Okal, E.A., Anderson, D.L.: Icarus **33** (1978) 514.
79Bat Bates, J.R., et al.: NASA Scientific and Technical Information Office; Reference Publication 1036 (1979).
79Goi Goins, N.R., Lazarewicz, A.R.: Geophys. Res. Lett. **6** (1979) 368.
79Nak Nakamura, Y., et al.: Proc. Lunar. Plant. Sci. Conf., 10th (1979) 2299.
79Tok Toksöz, M.N.: Rev. Geophy. Space Phys. **17** (1979) 1641.
80Bin Binder, A.B.: Geophys. Res. Lett. **7** (1980) 707.
80Vos Vostreys, R.W.: NASA Goddard Space Flight Center, Greenbelt, Maryland, NSSDC/WDC-A-R&S 80-11 (1980).
81Dzi Dziewonski, A.M., Anderson, D.L.: Phys. Earth Planet. Int. **25** (1981) 297.
81Goi Goins, N.R., et al.: J. Geophys. Res. **86(B6)** (1981) 5061.
81Yod Yoder, C.F.: Phil. Trans. R. Soc. Lond. A. **303** (1981) 327.
82Ksa Ksanfomaliti, L.V., et al.: Pisma Astron. Zh. **8** (1982) 444 (in Russian, English translation in: Sov. Astron. Lett. **8** (1982) 241).
82Nak Nakamura, Y. et al.: J. Geophys. Res. **87** (1982) Supp. A117.
83Dzi Dziewonski, A.M., Woodhouse, J.H.: J. Geophys. Res. **88** (1983) 3247.
83Mor Moroz, V.I.: In: Hunten, D.M. et al., editors, Venus, University of Arizona Press, Tucson, AZ, (1983) 1143.
83Nak Nakamura, Y.: J. Geophys. Res. **88** (1983) 677.
83Zha Zharkov, V.N.: The Moon and the Planets **29** (1983) 139.
84Lb Landolt-Börnstein, NS, Vol. V/2a (1984).
85Bin Binder, A.B., Oberst, J.: Earth Planet. Sci. Lett. **74** (1985) 149.
85Shi Shirley, J.B.: Earth Planet. Sci. Lett. **76** (1985/86) 241.
87Obe Oberst, J.: J. Geophys. Res. **92 (B2)** (1987) 1397.
88Mel Melosh, H.J., McKinnon, W.B.: In: Vilas, F. et al., editors, Mercury, University of Arizona Press, Tucson, AZ, (1988) 794.
89Obe Oberst, J.: PhD Thesis, The University of Texas at Austin, Austin, TX, (1989) 136.
91Ken Kennett, B.L.N., Engdahl, E.R.: Geophys. J. Int. **105** (1991) 429.
91Obe Oberst, J., Nakamura, Y.: Icarus **91** (1991) 315.
91Phi Philips, R.J.: In: LPI/TR-91-02, pp. 35-38, Lunar and Planet. Inst., Houston, TX (1991).
91Spo Spohn, T.: Icarus **90** (1991) 222.
92Gol Golombek, M.P., et al.: Science **258** (1992) 979.
92Sny Snyder, C.W., Moroz, V.I.: In: Kieffer, H.H. et al., editors, Mars, University of Arizona Press, Tucson, Arizona, (1992) 71.
92Zha Zharkov, V.N.: In: Barsukov, V.L. et al., Venus Geology, Geochemistry, and Geophysics, The University of Arizona Press, Tucson, Arizona, (1992) 233.
93Sto Stofan, E.R., et al.: Worksh. on Advanced Technologies for Planetary Instruments, Lunar and Planetary Inst., Houston, TX, part 1, 23-24 (1993).
96Gud Gudkova, T., Zharkov, V.N.: Planet. Space Sci. **44** (1996) 1223.
96Moc Mocquet, A., et al.: Planet. Space Sci. **44** (1996) 1251.
97Fol Folkner, W.M., et al. : Science **278** (1997) 1749.
97Soh Sohl, F., Spohn, T.: J. Geophys. Res. **102 (E1)** (1997) 1613.
99Aa The Astronomical Almanac for the Year 2000, Nautical Almanac Office, US Naval Observatory, Washington, DC, USA, and HM Nautical Almanac Office, London, GB (1999).

00Dav Davies, M.E., Colvin, T.R.: J. Geophys. Res. **105 (E8)** (2000) 20,277.
00Kha Khan, A., et al.: Geophys. Res. Lett. **27** (2000) 1591.
01Smi Smith, D. E., et al.: J. Geophys. Res. **106** (2001) 23,689.
01Wil Williams, J.G., et al.: J. Geophys. Res. **106 (E11)** (2001) 27,933.
02Bor Bormann, P., et al.: Chapter No. 3, In: Bormann, P., editor, IASPEI New Manual of Seismological Observatory Practice, GeoForschungsZentrum Potsdam, Vol. 1, (2002).
02Gol Golombek, M.P.: Lunar Planet. Sci. Conf., XXXIII, Abstract 1244.
02Wat Watters, T.R. et al.: Geophys. Res. Lett. **29** (2002) 1542.
03Dra Dragoni, M., Piombo, A.: Phys. Earth Planet. Int. **135** (2003) 161.
03Log Lognonné, P., et al.: Earth Planet. Sci. Lett. **211** (2003) 27.
03Log2 Lognonné, P., et al.: Geophys. Res. Abstr. **5** (2003) 11183.
03Smi Smith, D. E., et al.: MGS-M-MOLA-5-MEGDR-L3-V1.0, NASA Planet. Data Syst., Greenbelt, MD. (2003).
03Sol Solomon, S.C.: Earth Planet. Sci. Lett. **216** (2003) 441.
03Van Van Hoolst, T.: Jacobs, C.: J. Geophys. Res. **108** (E11), doi:10.1029/2003JE002126 (2003).
04Nak Nakamura, Y.: Apollo Passive seismic Experiment Long-Period Event Catalog, rev. 0704; available online at ftp://ftp.ig.utexas.edu/pub/PSE/catsrepts/levent.0104 (2004).
04Gud Gudkova, T.V., Zharkov, V.N.: Phys. Earth Planet. Int. **142** (2004) 1.
05Bul Bulow, R., et al.: J. Geophys. Res. **110** E10003, doi:10.1029/2005JE002414 (2005).
05Gar Garcia, R., et al.: Geophys. Res. Lett. **32** L16205, doi:10.1029/2005GL023558 (2005).
05Nak Nakamura, Y.: J. Geophys. Res. **110,** doi:10.1029/2004JE002332 (2005).
05Soh Sohl, F., et al.: J. Geophys. Res. **110** E12008, doi:10.1029/2005JE002520 (2005).
05Zha Zharkov, V.N., Gudkova, T.V.: Sol. Syst. Res. **39** (2005) 343.
06Bus Buske, M.: Dreidimensionale thermische Evolutionsmodelle für das Innere von Mars und Merkur, Dissertation, Univ. Göttingen, 201 pp (2006).
06Che Chenet, H., et al.: Earth Planet. Sci. Lett. **243** (2006) 1.
06Cmt The Global Centroid Moment Tensor Project, available online at: www.globalcmt.org, (2006).
06Fro Frohlich, C., Nakamura, Y.: Icarus **185** (2006) 21.
06Gag Gagnepain-Beyneix, J., et al.: Earth Planet. Sci. Lett. **159** (2006) 140.
06Kna Knapmeyer, M., et al.: J. Geophys. Res. **111** E11006, doi:10.1029/2006JE002708 (2006).
07Bul Bulow, R., et al.: J. Geophys. Res. **112** E09003, doi:10.1029/2006JE002847 (2007).
07Dro Drossart, P., et al.: Planet. Sp. Sci. **55** (2007) 1653.
07Mei Meissner, R.: Deutsche Geophys. Ges. Mitteilungen, No. 3/2007 (2007) 18-19.
07Sei Seidensticker, K.J., et al.: Sp. Sci. Rev. **128** (2007) 301.
08Mel Melosh, H.J.: Nature **452** (2008) 820.
08Riv Rivoldini, A., et al.: The interior structure of Mercury and its core sulfur content; submitted to Icarus (2008).
08Van Van Hoolst, T.: personal communication (email of 22. May 2008).